An Experimental Study of Fine Filaments NbTi Strand for Fast Cycled Magnets

U. Gambardella, F. Alessandria, G. Bellomo, P. Fabbricatore, S. Farinon, M. Holm, G. Iannone, B. Karlemo, H. Mueller, R. Musenich, D. Pedrini, A. Saggese, M. Sorbi, and G. Volpini

***Abstract*—The Italian Institute for Nuclear Physics is working on the development of fast cycled dipoles for the Facility for Antiproton and Ion Research SIS300 synchrotron at Gesellschaft für Schwerionenforschung, Darmstadt. In this framework the development of high current and low ac loss superconducting wires is an important step of the R&D. The main technique to attain these features is to develop fine filaments for the strands and to design suitable resistive barriers among filament islands within the strands. In this paper, we study a newly developed wire in terms of critical currents and ac losses. The critical current is obtained from magnetization cycle and direct transport current. The ac loss mechanisms caused by the interfilament electromagnetic coupling is related to the $\rho_{\rm et}$, the transverse resistance between adjacent filaments. We measure $\rho_{\rm et}$ through ac susceptibility technique.**

***Index Terms*—Accelerator magnets, magnetic losses, multifilamentary superconductors, niobium-titanium, superconducting magnets.**

I. Introduction

THE DEVELOPMENT of fast cycled magnets requires the use of low losses wires to keep low temperature dissipations at acceptable levels. In the past, a similar superconducting wire was developed within the R&D efforts for the SSC accelerator project [1]. Despite some good results, the process previously developed does not appear easily reproducible, and industrial scale production cannot be guaranteed. INFN and GSI in the framework of DIpoli SuperCOnduttori RApidamente Pulsati (DISCORAP) project, further to the realization of a fast ramped SIS300 dipole prototype [2], [3], also carried out a wire development program to manufacture a low loss wire for this application [4]. The development program is made of three steps: the first layout of the wire, which was used in the DISCORAP dipole, is made of 2.5 μm (geometrical) fine filament with CuMn resistive barriers, manufactured at Luvata Pori; a 2nd generation wire, also manufactured at Luvata Pori, has different CuMn barrier layout, which is being used in the Cluster of Research Infrastructures for Synergies in Physics (CRISP) European project; a 3rd generation wire will have a reduced filament size, 2 μm, and is under manufacture at EAS Bruker. The need of a 2nd generation wire comes out from manufacturing assessments of long (industrial) production of a fine filament NbTi wire (1st generation) before achieving reliability to make a step further.

In this paper we summarize the properties of the 2nd generation wire mainly in terms of its transport properties, magnetic hysteresis and ac losses. In Section II we describe the main improvements in designing the wire layout, and in Section III results of the low temperature measurements are discussed, also in connection of a numerical model concerning the ac losses computation. Finally in Section IV conclusions are drawn.

II. Wire Geometrical Features

The 2nd generation wire has to fill the gap between the performances achieved in the first generation wire and the target values set according the design of the SIS300 model dipole. Namely we expect to increase the critical current density $J_{\rm c}$ as well as the transverse resistance $\rho_{\rm et}$. Two main strategies have taken place: the increase of the filament number (increasing the subelements number from 690 to 714) and the increase of subelements having CuMn (Cu 0.5wt% Mn) barriers. In Fig. 1 it is reported the SEM pictures concerning the wires of 1st generation (a and b) and 2nd generation (c and d), respectively. Even at different magnifications, a lower filament distortion may be recognized when passing from the 1st to the 2nd generation wire. Each subelement has its own CuMn matrix, and additional CuMn barriers around some adjacent subelements, make a special barrier against coupling currents. Several layouts of these special subelements have been analyzed numerically [5] in order to optimize the increase of $\rho_{\rm et}$ with respect to the first generation wire, while keeping good cryogenic stability of the wire. The selected layout should lead to a 50% increase in $\rho_{\rm et}$ with respect to the 1st generation wire.

Manuscript received July 17, 2013; accepted August 30, 2013. Date of publication September 16, 2013; date of current version October 14, 2013. This work was supported in part by the E.U.-Research Infrastructure Activity under the FP7 program CRISP (Grant 283745), Work Package 5. The work of G. Iannone was supported in part by PON Ricerca e Competitività 2007–2013 under Grant agreement PONa3_00007.

U. Gambardella and G. Iannone are with INFN-Sezione di Napoli, Gruppo Collegato di Salerno, University of Salerno, 84084 Fisciano, Italy (e-mail: gamba@sa.infn.it).

F. Alessandria, G. Volpini, and D. Pedrini are with INFN-LASA, 20090 Segrate, Italy.

M. Sorbi and G. Bellomo are with the Physics Department, Milan University and INFN-LASA, 20090 Segrate, Italy.

P. Fabbricatore, S. Farinon, and R. Musenich are with INFN Sez. di Genova, 16146 Genova, Italy.

M. Holm and B. Karlemo are with Luvata Pori Oy, 28101 Pori, Finland.

H. Mueller is with GSI, 64291 Darmstadt, Germany.

A. Saggese is with CNR-SPIN, Physics Department, University of Salerno, 84084 Fisciano, Italy.

Color versions of one or more of the figures in this paper are available online at http://ieeexplore.ieee.org.

Digital Object Identifier 10.1109/TASC.2013.2281465

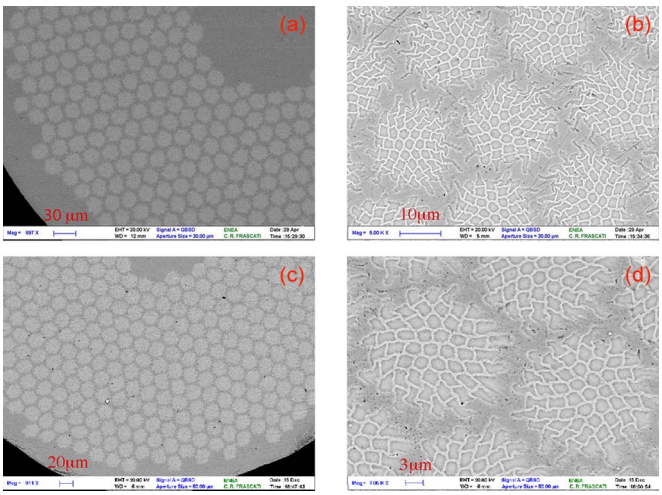

Fig. 1. SEM pictures of the first-generation wire (a, b) and the second-generation wire (c, d).

TABLE I
COMPARISON BETWEEN WIRES MAIN FEATURES

	1st generation	2nd generation[a]
total no. of filaments	37 950	39 270
α factor (Cu-non Cu ratio)	1.75	1.61
RRR value	>100	>100
geometrical filament size	2.5 µm	2.5 µm
nominal twist pitch	6.6 mm	6.6 mm
strand diameter (2r)	0.821 mm	0.821 mm

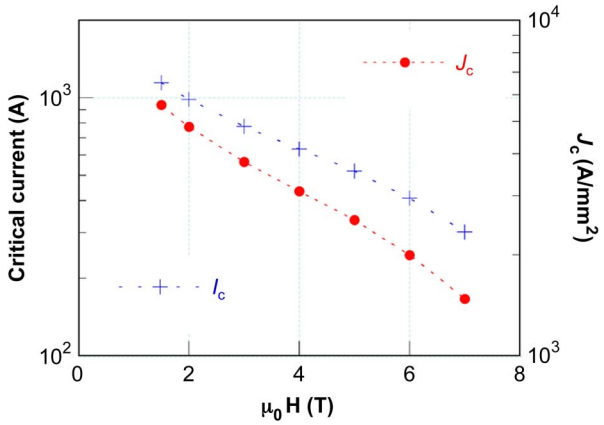

Fig. 2. Direct current transport measure at 4.2 K of the second-generation wire as a function of the applied magnetic field.

III. EXPERIMENTAL PERFORMANCE OF THE WIRE

The 2nd generation wire has been characterized against its transport properties with direct current carrying transport measurements and magnetic measurements, both *dc* and *ac*.

In Table I some wire features between the 1st and 2nd generation wire are compared.

In Fig. 2 the critical current behavior as a function of the applied magnetic field is shown. The wire achieved at 4.2 K a $J_c = 2541\ \mathrm{A/mm^2}$ at 5 T, with an improvement of less than 6% with respect of the 1st generation wire [4]. This is in agreement to the increased superconducting volume fraction, $\lambda = 1/(1+\alpha)$, of 5.4% for this wire. For all the field strength values, also the n index in the 2nd generation wire resulted always higher than the corresponding one in the 1st generation wire. This is again consistent with the reduced filament distortion observed in SEM analyses.

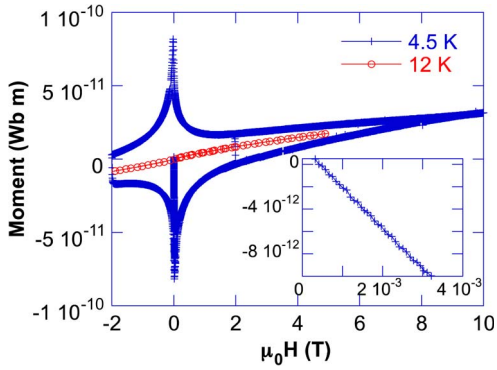

Fig. 3. Hysteresis cycle measure of the second-generation wire as a function of the applied magnetic field at 4.5 K (superconducting) and 12 K (normal).

In Fig. 3 the magnetic moment m of the 2nd generation wire as a function of the applied magnetic field is shown, at 4.5 K and 12 K. The measurement is carried out with a VSM magnetometer, where a length $l = 11.8$ mm of wire is shaped in a small ring having a 5 mm diameter. The sample is arranged in a way that the ring is coaxial to the external field and to the vibration direction. In this measure are included all the irreversible and reversible magnetization components, M_{irr} and M_{rev}, respectively, of the composite wire, i.e. the NbTi and the CuMn. Further the standard deconvolution, which let us to extract M_{irr} and M_{rev} in the curve in Fig. 3, we also could compare the M_{rev} with the 12 K measurements, neglecting the CuMn temperature corrections. M_{irr} is useful to compute specific features of the wire, such as the effective filament diameter d_{eff} [6]:

$$M_{irr}(B) = \frac{2}{3\pi}\mu_0(1+\alpha)J_c(B,T)d_{eff} \tag{1}$$

where μ_0 is the magnetic permeability in vacuum. At 5 tesla a $d_{eff} = 3.5\ \mu$m and $d_{eff} = 3.2\ \mu$m is found, respectively neglecting and taking into account of the self-field contribution in the I_c measure. It is worth noting that the value of d_{eff} is larger than the nominal value and, in addition, it is not constant as a function of the applied magnetic field. The first occurrence may be ascribed to the fact that the (1) is a simple model based on a single round filament computation, which is different from the actual manufactured strand (multiple filaments, filament distortion, etc.). This result has to be compared to $d_{eff} = 3\ \mu$m in the 1st generation wire [7], computed by considering the self-field correction in the I_c transport measure. From the irreversible values of the magnetization near H_{c2} we can also derive the Ginzburg-Landau constant $\boldsymbol{\kappa}$ [8]:

$$\frac{dM_{irr}}{dH} = 2 \cdot \frac{1}{2\kappa^2(T) - 1)\beta_A} \tag{2}$$

where the Abrikosov constant in a triangular array of fluxons $\beta_A \approx 1.16$ and the factor 2 comes from the demagnetization factor, N = 1/2 for a round wire in transverse magnetic field. In our case we estimated a value $\boldsymbol{\kappa} = 39$.

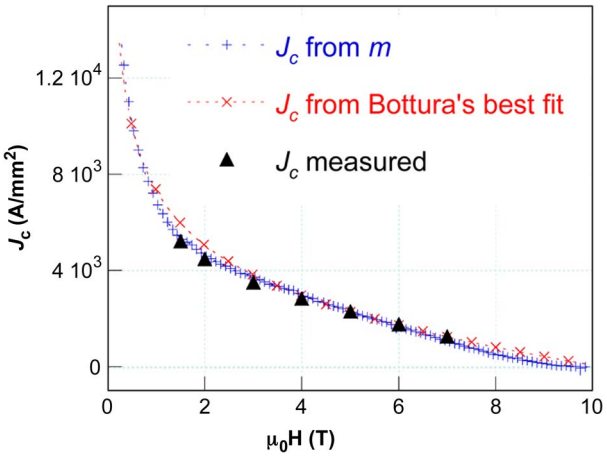

Fig. 4. Critical current comparison, magnetic vs. transport in the second-generation wire as a function of the applied magnetic field, at 4.5 K.

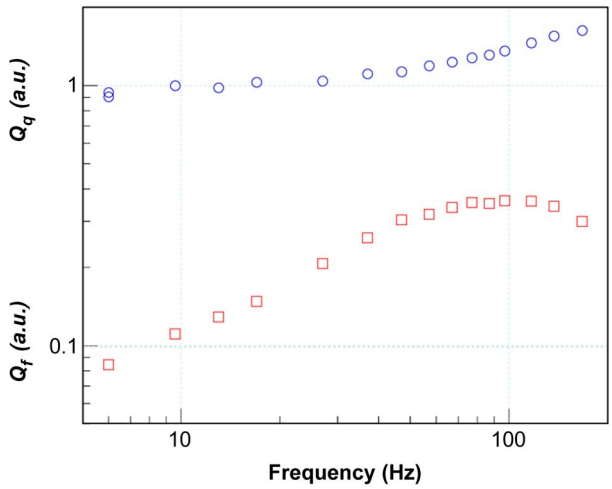

Fig. 5. Frequency behavior of the quantities Q_f (□) and Q_q(o). A characteristic frequency of about 90 Hz is found.

The first virgin moment of the sample at very low field is also shown in the inset of Fig. 3. This represents the Meissner state of the superconducting part of the composite wire, whose slope is straight connected to the superconducting volume fraction of the wire. If we crudely assume a round wire model the slope corresponds to a s/c volume filling factor $\lambda = 0.31$, to be compared to the nominal $\lambda = 0.38$. Both filament distortion and magnetic field penetration in the fine filaments may explain this discrepancy.

The critical current density $J_c(B)$, computed assuming $d_{eff} = 3.5\ \mu$m, from the magnetization of the sample is shown in Fig. 4 (+). There are also shown the transport measurements (▲), corrected for the temperature difference, and the best fit curve (×) computed at 4.5 K by using the Bottura's phenomenological relation [9] (the parameters are $C_0 = 31.4$, $\alpha = 0.63$, $\beta = 1$, $\gamma = 2.3$, $T_{c0} = 9.2$, $B_{c20} = 14.5$). As noted before, the d_{eff}, which actually comes from the ratio

$$d_{eff} = \frac{3\pi}{2\mu_0}\frac{m}{I_c l} \tag{3}$$

is not constant as a function of the applied magnetic field. This implies that the $J_c(H)$ curve (derived from m) fits the experimental measurements just at the point where d_{eff} has been evaluated (i.e. at 5 T in our picture).

Finally we also investigated the ac properties of the wire by using the ac susceptibility technique [10]. In the ac technique, the out-of-phase V_q and in-phase signals V_f measured by the lock-in, are directly proportional to the ac susceptibility components, χ' (real) and χ'' (imaginary), through a constant that includes the the pick-up coil geometrical factor. The V_f is physically related to the energy coupling loss. This energy per cycle and per unit volume, W, in a composite strand under a transverse sinusoidal field $B_{ac} = B_0 sin(\omega t)$ of angular frequency $\omega = 2\pi f$ and peak value B_0 is [6]

$$W = \chi_0 \frac{B_0^2}{\mu_0}\pi\frac{\omega\tau}{1+\omega^2\tau^2} \tag{4}$$

where χ_0 is the external susceptibility, under the condition of perfect screening. The characteristic time constant, τ, is directly proportional to the square of the twist pitch, L, and inversely proportional to the transverse resistivity ρ_{et}:

$$\tau = \frac{\mu_0}{2\rho_{et}}\left(\frac{L}{2\pi}\right)^2. \tag{5}$$

This model is valid when the full saturation condition is fulfilled, thus the measurements were performed in the presence of a static magnetic field $B_{ext} = 0.2$ T, transverse to the filament direction. From the complete V_q and V_f behavior as a function of the temperature, we can compute the quantities $Q_f = [V_f(4\ \text{K}) - V_f(10\ \text{K})]/(B_0 f)$ and $Q_q = [V_q(4\ \text{K}) - V_q(10\ \text{K})]/(B_0 f)$. In Fig. 5 it is reported the $Q_{p,f}$ value as a function of the ac frequency f, being $B_0 = 10^{-3}$ T. The meaning of Q_q is related to the shielding features of the sample, while Q_f is related straight to the wire dissipations under ac regime [10]. The peak on the Q_f curve is found at the characteristic frequency $f \approx 90$ Hz, corresponding to $\tau \approx 1.77\ 10^{-3}$ s. Finally, according to (5), this τ value leads to the transverse resistivity: $\rho_{et} \approx 3.91\ 10^{-10}\ \Omega$m. In the 1st generation wire we measured a $\rho_{et} = 3.0\ 10^{-10}\ \Omega$m by using the same technique [7].

The measured value of the transverse resistivity can be also compared to the numerical simulation made on the wire geometry, by using the simple interpretative model based on the work performed by Duchateau, Turck and Ciazynski [11]. We assume that the time scale of the varying field dB/dt is much larger than the wire characteristic time τ. Under this condition there is no difference between the internal and the external field, and the voltage applied to a filament placed at a position (x, y) in the wire cross section is:

$$V(x) = \frac{Lx}{2\pi}\left(\frac{dB}{dt}\right). \tag{6}$$

Here the dB/dt field is directed along the x direction, thus we can find the correct current distribution by applying this condition to the filaments and solving the static electric problem with the Laplace equation. This should be done to the whole wire cross section, but, as it is inconvenient to model

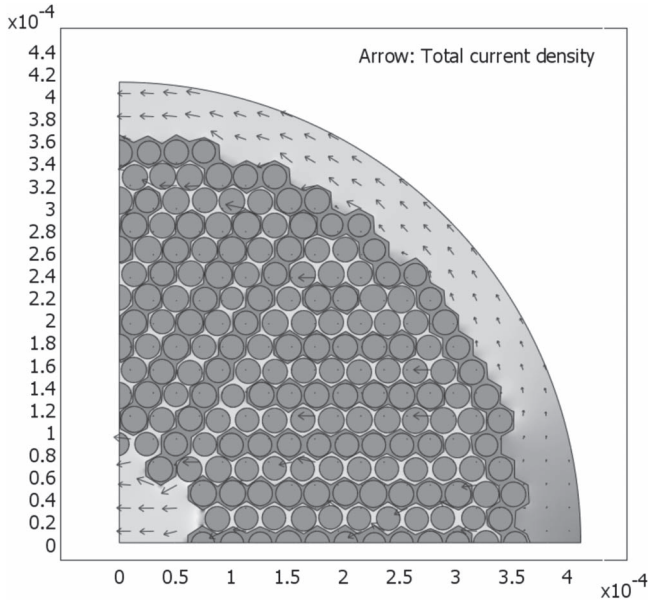

Fig. 6. Numerical computation of the current flow in the second-generation wire.

39,270 filaments, we only consider the subelements applying the conditions straight to them. This approximation would be reasonable, being the filaments in the bundles surrounded by CuMn matrix, so that the coupling currents mainly flow through the parts of the Cu matrix surrounding the bundles. The obtained current distribution for the strand is shown in Fig. 6. By using the computed current distribution, we can calculate the electrical dissipation P per unit volume integrating the local calculated electric field $E(x, y)$ and the local current density $J(x, y)$ over the cross section and dividing by the whole cross section S:

$$P = \frac{1}{S} \int_S E(x, y) J(x, y)\, dx\, dy. \tag{7}$$

From the total dissipated power, the time constant can be derived through [6]:

$$\tau = \frac{\mu_0 P}{2\dot{B}^2}. \tag{8}$$

From this numerical analysis we have found $\tau = 1.19\, 10^{-3}$ s, that is a characteristic frequency $f = 130$ Hz, corresponding to a $\rho_{et} = 5.8\ 10^{-10}\ \Omega$m, higher than the measured one. The same occurrence was found in 1st generation wire, where the computed value of $\rho_{et} = 4.6\ 10^{-10}\ \Omega$m was again larger than the experimentally measured $\rho_{et} = 3.0\ 10^{-10}\ \Omega$m. This discrepancy is again ascribed to the used model, which is very far from the real morphology reported in Fig. 1. In fact the presence of strong deformation may easily reduce the performance of barriers, lowering the transverse resistance.

IV. Conclusion

The 2nd generation wire aimed to achieve a low losses standard manufacturing process, developed in the framework of the INFN fast ramped dipole program, has been characterized. This wire is being used for the low loss Rutherford cable manufacture in the Eu-CRISP project to realize a second winding of the SIS300 fast ramped dipole. This 2nd generation wire actually showed an increase of the critical current density as well as a higher transverse resistivity when compared to the 1st generation wire. This results mark a step ahead through the manufacture of low losses wires required for fast cycled magnets.

Acknowledgment

The authors thank A. Ferrentino (University of Salerno) for the technical support. The authors also thank A. Rufoloni (ENEA Frascati) for the SEM analysis.

References

[1] H. Kanithi, W. Wiegert, P. Valaris, M. D. Sumption, and E. W. Collings, "Current density and magnetization of fine filamentary NbTi superconductors," in *Supercollider 5*, P. Hale, Ed. New York, NY, USA: Plenum, 1994.

[2] P. Fabbricatore, S. Angius, G. Bellomo, P. Fabbricatore, S. Farinon, U. Gambardella, R. Marabotto, R. Musenich, R. Repetto, M. Sorbi, and G. Volpini, Technical design report of the superconducting dipole for fair SIS300, Natl. Inst. Nucl. Phys., Bologna, Italy, Tech. Design Rep. INFN-13-06-GE. [Online]. Available: http://www.lnf.infn.it/sis/preprint/pdf/getfile.php?filename=INFN-13-06-GE.pdf

[3] P. Fabbricatore, F. Alessandria, G. Bellomo, U. Gambardella, S. Farinon, R. Marabotto, R. Musenich, M. Sorbi, and G. Volpini, "The construction of the model of the curved fast ramped superconducting dipole for FAIR SIS300 synchrotron," *IEEE Trans. Appl. Supercond.*, vol. 21, no. 3, pp. 1863–1867, Jun. 2011.

[4] G. Volpini, F. Alessandria, G. Bellomo, P. Fabbricatore, S. Farinon, U. Gambardella, J. Kaugerts, G. Moritz, M. Sorbi, and M. N. Wilson, "Low-loss NbTi Rutherford cable for application to the SIS-300 dipole magnet prototype," *IEEE Trans. Appl. Supercond.*, vol. 18, no. 2, pp. 997–1000, Jun. 2008.

[5] G. Volpini, F. Alessandria, G. Bellomo, M. Sorbi, P. Fabbricatore, S. Farinon, R. Musenich, U. Gambardella, J. Kaugerts, G. Moritz, and M. N. Wilson, "Low loss wire design for the DISCORAP dipole," in *Proc. WAMSDO Workshop*, Geneve, Switzerland, May 19–23, 2008, CERN.

[6] M. N. Wilson, *Superconducting Magnets*. Oxford, U.K.: Oxford Univ. Press, 1983.

[7] G. Volpini, F. Alessandria, G. Bellomo, P. Fabbricatore, S. Farinon, U. Gambardella, R. Musenich, M. Sorbi, B. Karlemo, and M. Holm, "Low loss Nb-Ti superconducting Rutherford cable manufacture for the SIS300 INFN model dipole," *IEEE Trans. Appl. Supercond.*, vol. 21, no. 3, pp. 3334–3337, Jun. 2011.

[8] M. Tinkham, *Introduction of Superconductivity*. New York, NY, USA: McGraw-Hill Inc., 1975.

[9] L. Bottura, "A practical fit for the critical surface of NbTi," *IEEE Trans. Appl. Supercond.*, vol. 10, no. 1, pp. 1054–1057, Mar. 2000.

[10] P. Fabbricatore, S. Farinon, S. Incardone, U. Gambardella, A. Saggese, and G. Volpini, "The transverse resistivity in S/C multifilament wires studied through ac susceptibility measurements," *J. Appl. Phys.*, vol. 106, no. 8, pp. 083905-1–083905-8, Oct. 2009.

[11] L. Duchateau, B. Turck, and D. Ciazynski, *Handbook of Applied Superconductivity*, B. Seeber, Ed. Bristol, U.K.: IoP Berkshire, 1998, p. 205.